Sensitivity of metabolic constraints for marine organisms to emission scenarios

Takamitsu Ito[1], Amy Weng[1], and Holt Thomas[1]

[1]School of Earth and Atmospheric Sciences, Georgia Institute of Technology, Atlanta, Georgia, U.S.A.

Key Points:

- Centennial decline of metabolic indices are examined under three emission scenarios using CMIP6 earth system models
- Effects of warming and deoxygenation together decrease the metabolic index in the northern extratropical oceans
- Emission scenarios significantly alter the magnitude of the changes while its spatial patterns are model-dependent

Corresponding author: Takamitsu Ito, taka.ito@eas.gatech.edu

Abstract

Marine ecosystem is influenced by multiple factors under the global warming. Increasing temperature raises the matabolic demand for oxygen, however, its supply declines as the concentration of dissolved oxygen decreases. Metabolic index is defined as the oxygen supply to demand ratio for a marine organism, quantitatively combining the effects of ocean warming and deoxygenation. A subset of the earth system models participating in the Coupled Model Intercomparison Project phase 6 (CMIP6) are used to calculate the century-scale changes in the metabolic index under three different scenarios. Under the most aggressive warming scenario, metabolic index can decline over 50% at northern extratropics including the US west coast. Overall magnitude of the change is dependent on the emission scenarios, whereas spatial patterns are model-dependent, in particular at low latitudes due to the large uncertainty in projected oxygen changes.

Plain Language Summary

Global warming changes many aspects of physical and chemical environments in the oceans. Direct observations have shown temperature increase and oxygen decrease for the past several decades, and climate models predict that these trends continue for this century. It is difficult to understand the impacts of multiple environmental factors on marine ecosystems. Recent theoretical advances combines temperature and oxygen to calculate the metabolic constraints of marine animals. Warming increases oxygen demand due to increasing metabolic rates, however, the supply of oxygen is decreasing. Metabolic index can be defined as the oxygen supply to demand ratio. This study delineates the two factors in the context of climate model projections of metabolic index for the 21st century under different socio-economic scenarios. Comparing four different models gives us a sense of uncertainty due to model structure. We find that warming and oxygen loss play approximately equal role in tightening the metabolic constraints, especially in the mid and high latitude northern hemisphere oceans including the US west coast. These regions exhibit more than 50% decline in the metabolic index under the "business-as-usual" emission scenario, but choosing less aggressive emission scenarios can significantly reduce the decline of metabolic index in these regions.

1 Introduction

The oceans are the dominant sink of excess heat under the global warming (Zanna et al., 2019) accounting for more than 90% of the Earth's energy imbalance (Cheng et al., 2017). The greatest temperature increase occurs at the surface while deep temperatures remain nearly unchanged due to the slow ventilation of deep waters relative to the timescale of the anthropogenic forcing. This contrast in the rate of warming increases the vertical density difference. Stronger vertical stratification tends to decrease the upper ocean mixing and reduce the vertical transfer of chemical properties. The temperature increase reduces the solubility of oxygen in the seawater, and the increased density stratification further weakens the vertical mixing of oxygen into the interior ocean. These two reinforcing mechanisms decrease the dissolved oxygen concentrations under transient warming scenarios (Matear et al., 2000; Keeling & Garcia, 2002; Keeling et al., 2010). Direct observations of dissolved oxygen show a significant decline during the last several decades (Helm et al., 2011; Schmidtko et al., 2017) in association with the observed increase in ocean heat content (Ito et al., 2017).

Increasing temperature and declining oxygen levels are two of the major ecosystem stressors under the warming climate (Gruber, 2011; Bopp et al., 2013). Rates of physiological processes typically depend on temperature. As temperature increases, animals' metabolic oxygen demands are expected to increase. In order for a marine habitat to be viable, the rate of oxygen supply must exceed the resting metabolic demand. Metabolic index (Φ) is defined as the oxygen supply to demand ratio for a marine organism, which quantitatively combines the effect of warming and oxygen loss (Deutsch et al., 2015).

$$\Phi = A_0 B^n \frac{pO_2}{exp(-E/k_B T)} \tag{1}$$

A_0 is a constant coefficient specific to individual species, and B is the body mass. pO_2 is the partial pressure of oxygen of the ambient water, and E (eV) is the temperature sensitivity parameter. k_B (eVK^{-1}) is the Boltzmann constant, and T (K) is the absolute temperature. If Φ is less than 1, the oxygen supply cannot meet the resting metabolic demand. Observed distribution of marine organisms require minimum metabolic index (Φ_{crit}) of 2 to 5 in order to support critical activities such as growth and reproduction, and the maps of $\Phi > \Phi_{crit}$ capture the patterns of observed marine habitats (Deutsch et al., 2015). Taking the logarithmic derivative of (1) the relative importance of warm-

ing and oxygen loss can be evaluated.

$$\frac{\delta\Phi}{\Phi} = \frac{\delta pO_2}{pO_2} - \frac{E}{k_B T^2}\delta T \tag{2}$$

For a given body mass (constant B), fractional changes in Φ is linearly dependent on pO_2 and temperature. In this framework, relative importance between the two environmental variables (pO_2 and T) is controlled by the empirically determined temperature sensitivity parameter (E). The magnitude of E varies from 0.3 to $1.0eV$ in published data (Deutsch et al., 2015) with the median of $0.6eV$. Larger values for this parameter indicate greater influence of temperature relative to pO_2. Surface waters are temperature dominated due to the air-sea gas transfer setting $pO_2 \sim pO_{2,air}$. Oxygen concentration below the surface mixed layer is controlled by the balance between the ventilation and the respiratory O_2 losses. Under increasing density stratification and weakened ventilation, subsurface pO_2 is predicted to decrease by shifting the balance towards teh respiratory O_2 losses. The reinforcing changes in pO_2 and T are predicted in the subsurface where significant decreases in pO_2 can occur.

The objective of this paper is to examine the centennial trends of the metabolic index as simulated by a subset of earth system models (ESMs) participating in the Coupled Model Intercomparison Project Phase 6 (Eyring et al., 2016) under different emission scenarios. Three future scenarios are considered; ssp126, ssp245 and ssp585 covering a wide range of fossil fuel emissions (Gidden et al., 2019). Four models are selected based on the availability of necessary output variables to calculate the metabolic index for pre-industrial control, historical and future scenario simulations; CanESM5 (Swart et al., 2019a, 2019b, 2019c, 2019d, 2019e, 2019f), CNRM-ESM2-1 (Sfrian et al., 2019; Seferian, 2018), GFDL-CM4 (Held et al., 2019; Guo et al., 2018) and IPSL-CM6A-LR (Boucher et al., 2018). The structure of this manuscript is as follows. Section 2 describes the model data analysis methods. Section 3 discusses the centennial changes of metabolic index, its breakdown into temperature and oxygen components, and its scenario dependence. Section 4 summarizes the results and discusses its implications.

2 Model Data Analysis Methods

The specific set of ESM simulations used in this study includes the pre-industrial control (piControl), historical simulation (historical) and future projections (ssp126, ssp245, and ssp585). Historical simulation covers from 1850 to 2015 and the ssp scenarios cover

from 2016 to 2100. The monthly means of ocean potential temperature (θ), salinity (S), and dissolved oxygen (O_2) are first re-gridded into global 2° longitude-latitude grid using bilinear interpolation. Subsequently the annual mean of each variables are calculated, and the model drift is removed from every grid point using the linear trend of piControl from 1850 to 2100. Drift correction is applied for each variable before the metabolic indices are computed.

Figure 1 evaluates the climatological O_2 at 200m depth over the period from 1980 to 2000, and model outputs are compared to the World Ocean Atlas 2018 (Garcia et al., 2018). The models capture the spatial variability reasonably well with the correlation coefficient of 0.93 to 0.94. These models can reproduce large scale gradients in O_2 where high latitude waters are relatively well ventilated, and the tropical thermocline is relatively depleted in O_2. The global median O_2 is 219μM for the observation (WOA2018), and the modeled values are 242μM for CanESM5, 217μM for CNRM-ESM2-1, 234μM for GFDL-CM4, and 218μM for IPSL-CM6A-LR. Supplementary Figure S1 shows the difference between the model and the observation. Interestingly, all models overestimate O_2 concentrations in the central and western tropical Pacific, and also overestimate it in the subpolar North Pacific. Besides these regions, the pattern of the mean-state biases differ from model to model without a common pattern. CanESM5 tends to overestimate the O_2 in all basins especially at high latitudes and in the western part of tropical basins. CNRM-ESM2-1 generally underestimates the O_2 in the tropical Atlantic and in the Southern Ocean, but it tends to overestimate in the North Pacific. This model also underestimates O_2 in the core of the tropical oxygen minimum zones (OMZs). GFDL-CM4 tends to overestimate O_2 in the Pacific basin with the exception of tropical pacific OMZ, where this model well captures the zonally elongated structure of the low-O_2 water there. This model also exhibits the least bias in the subpolar North Atlantic. IPSL-CM6A-LR generally overestimate O_2 in the tropical Pacific but underestimates in the Southern Ocean.

Potential temperature (θ) is another important variable for the calculation of the metabolic index. The models capture the spatial variability of potential temperature at 200m significantly better than oxygen with the correlation coefficient of 0.96 to 0.99 (see also, Supplementary Figure S2). The global median θ at 200m depth is 11.2°C for the observation (WOA2018), and the models are 11.6°C for CanESM5, 11.1°C for CNRM-ESM2-1, 9.7°C for GFDL-CM4, and 11.1°C for IPSL-CM6A-LR. While some models show

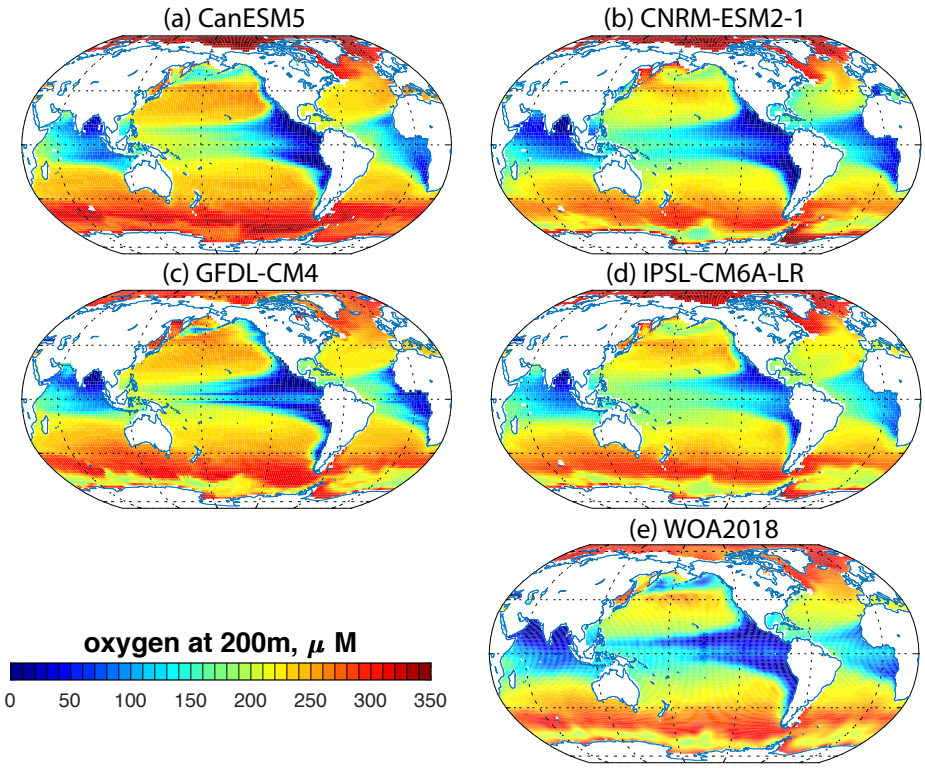

Figure 1. Model-Observation comparison of climatological, annual mean dissolved oxygen at 200m depth. (a-d) The plotted values are based on drift-corrected oxygen concentration based on the historical simulation. Climatology is based on the 20-year averages between 1980 to 2000 for the model data. (e) Climatological annual oxygen concentration based on the World Ocean Atlas 2018.

median θ closer to the observation than others, spatial pattern of model biases show similar order of magnitudes among all the models (Supplementary Figure S3). In some models, these biases compensate one another to exhibit the global median temperature that is very close to the observation. All models underestimated potential temperature in the subtropical South Pacific from 10°S to 30°S. GFDL-CM4 generally underestimated the subsurface potential temperature in all basins with the exception of the tropical Indian Ocean. In the subpolar North Atlantic, however, GFDL-CM4 better represents the thermal structure. Other models tend to exhibit a cold bias in the south of Greenland, reflecting overly zonal structure of the North Atlantic Current, as seen in earlier (CMIP5) versions of ESMs (Tagklis et al., 2017). With these biases in mind, we proceed to calculate the metabolic index in the next section.

3 Centennial Changes of Metabolic index

pO_2 is calculated as the ratio between the oxygen concentration (O_2) and the Henry's law coefficient for oxygen saturation following Garcia and Gordon (1992). In order to calculate the centennial trend, we take the 20-year average over 2080 to 2100 in the scenario runs and subtract the 20-year average over 1980 to 2000 from the historical simulation. The mean state of the metabolic index, according to (1), generally takes its minimum value in the tropics and increases towards high latitudes. This is caused by the poleward increase in oxygen concentration (and pO_2) and decrease in temperature, both contributing to the poleward increase in the metabolic index (Φ). Typically the critical condition ($\Phi = \Phi_{crit}$) occurs somewhere in the mid-latitudes, setting the equatorward edge of the organism's habitat. Increasing temperature and/or decreasing oxygen generally indicate the poleward migration of this critical latitude.

Figure 2 shows the centennial change of Φ at 200m in percent from each of the four ESMs. GFDL-CM4 did not include the ssp126 scenario at the time of the writing of this manuscript. Figure 2 is based on the median temperature sensitivity ($E = 0.6eV$). The depth of 200m is chosen to capture the upper-ocean environment, but below the base of surface mixed layer for most of the ocean regions. Temperature sensitivity parameter (E) varies over 0.3 to $1.0eV$ resulting in $\sim \pm 50\%$ change in the temperature contribution of the change. Temperature effect generally decreases the metabolic index as the seawater warms up.

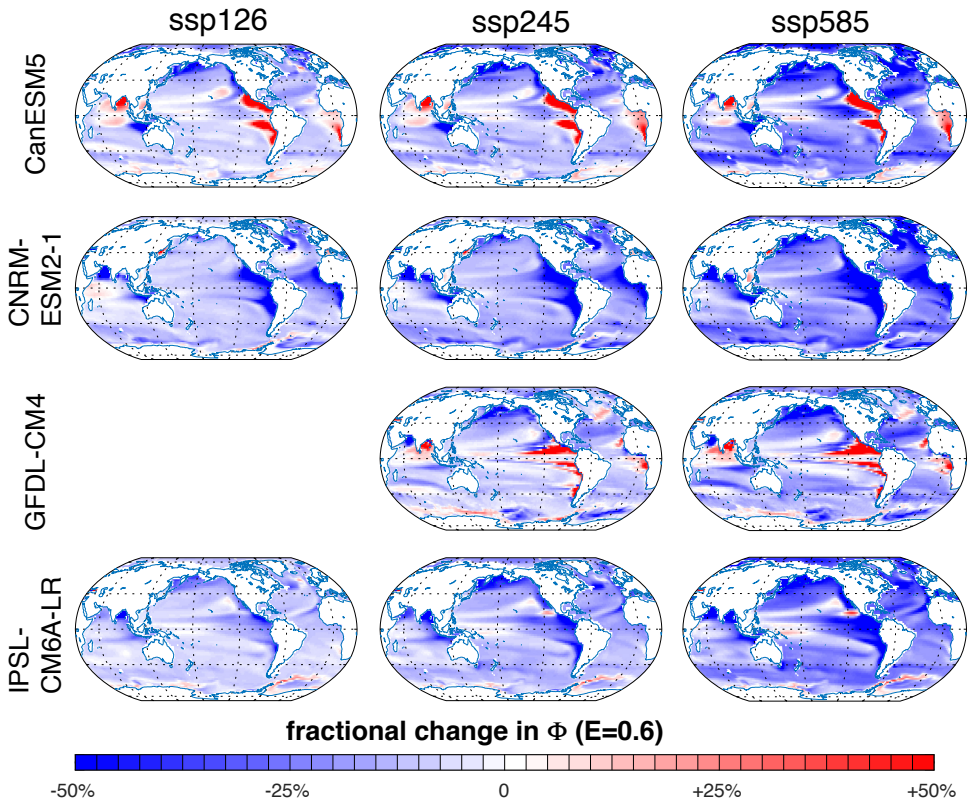

Figure 2. Centennial change of metabolic index at 200m depth with the median temperature sensitivity ($E = 0.6eV$). The centennial change is evaluated by the difference between the two periods; 1980-2000 and 2080-2100. Consistent color shading is used for all panels. From left to right, each column shows the results from ssp126, ssp245 and ssp585 scenario runs. From top to bottom, each raw shows the results from difference ESMs; CanESM5, CNRM-ESM2-1, GFDL-CM4, and IPSL-CM6A-LR.

In general, the metabolic indices are decreasing in all emission scenario (Figure 2). In many regions the magnitude of the decline exceeds 50% under the ssp585 scenario. The strongest decrease occurs in some regions of the northern extratropics especially in the California coast, the northern North Atlantic, the western subpolar North Pacific. Comparing difference emission scenarios, the scenario dependence occurs mainly in the magnitude of the change, and the spatial patterns are generally set by the specific model structure. As the degree of global warming intensifies from ssp126 to ssp585, the decrease of metabolic indices gets greater in magnitude across all the models.

Models disagree in the sign of change in some parts of the tropics. CanESM5 and GFDL-CM4 show an increase in metabolic indices in the eastern tropics including Pacific, Atlantic and Indian basins. In contrast, CNRM-ESM2-1 and IPSL-CM6A-LR show decreases in the eastern tropics. In these regions, the increase in metabolic indices are caused by the increase in pO_2 (Figure 3). The oxygen contributions are calculated according to the first term in the RHS of (2). Temperature of seawater increases in these regions (see Figure S4) but the oxygen increase dominates over the thermal effect at low latitudes.

Increased stratification and shallower mixed layer depths will weaken the ocean ventilation and reduce subsurface O_2 in the subduction regions at mid and high latitudes (Keeling et al., 2010; Matear et al., 2000). However, there are several other factors that affect the centennial O_2 trends (Oschlies et al., 2018). Shifts in atmospheric winds can alter the ocean circulation and the ventilation of thermocline. Increased stratification can also reduce the vertical nutrient supply, potentially weakening the biological productivity and export of organic matter. Reduced respiration tends to leaves behind subsurface O_2, leading to an increase in pO_2. Furthermore, increased stratification may weaken the overturning circulation, weakening the upwelling deep water into the tropical thermocline (Gnanadesikan et al., 2007), leading to an reduction in the age of water and pO_2 increase in the tropical thermocline. The combinations of these factors together control the sensitivity of pO_2 in the tropical thermocline. The superposition of multiple mechanisms makes the attribution challenging (Takano et al., 2018). Individually, each model shows consistent change for all three basins for all scenarios. Thus, the tropical oxygen changes are largely model-dependent, and the disagreement between the models highlights significant uncertainty in the low latitudes.

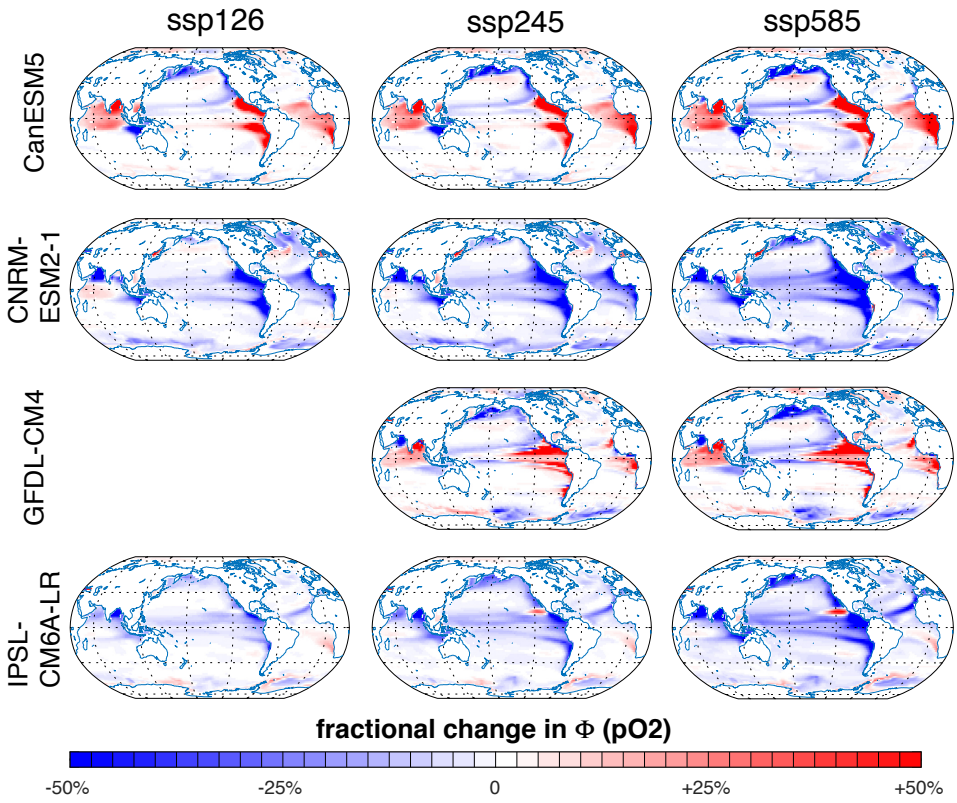

Figure 3. Oxygen contribution to the centennial change of metabolic index at 200m depth as the difference between the two periods; 1980-2000 and 2080-2100. From left to right, each column shows the results from ssp126, ssp245 and ssp585 scenario runs. From top to bottom, each raw shows the results from difference ESMs; CanESM5, CNRM-ESM2-1, GFDL-CM4, and IPSL-CM6A-LR.

4 Discussions and Conclusions

Metabolic demand for O_2 increases as the ocean absorbs excess heat and the temperature rises. Climate models predict the decline of dissolved oxygen and its partial pressure in the subsurface waters (Bopp et al., 2013; Keeling et al., 2010) while significant uncertainty still remains about the models' ability to reproduce observed mean states, variability and trends from the past several decades (Cabre et al., 2015; Eddebbar et al., 2017; Stramma et al., 2012). There is a general tendency for ESMs to underestimate the oxygen trends relative to the historic data (Oschlies et al., 2017). With those limitations in mind, a subset of the CMIP6 models are used to assess the projected centennial change in metabolic index for the 21st century. Figure 4 summarizes our results. In the zonal mean sense, the thermal and oxygen contributions together drives the decrease of metabolic index poleward of 35°N and 35°S. The strong oxygen decline in northern extratropical latitudes combines with the effect of temperature increase to drive the major decrease there. Eastern boundary upwelling region of the US west coast is another high impact areas where the temperature increase and oxygen decline reinforce one another. For the case of E=0.6eV, relative contributions from pO_2 and T are approximately the same in these regions. All models are in agreement that the net change in Φ can reach and exceed 50% decline under the ssp585 scenario, which can be avoided in the case of the ssp126 or ssp245 scenarios. The northern extratropics including the California coast can be the hot spots of the regional ecological impacts because of the critical condition, $\Phi \sim \Phi_{crit}$, typically occurring close to these regions. In another words, the strongest decline in metabolic index are predicted to occur where the ecosystem is already close to the critical threshold.

The changes in Φ are uncertain at low latitudes. Models generally have difficulty reproducing the mean state and/or variability of observed O_2 in the tropical thermocline (Cabre et al., 2015; Stramma et al., 2012; Oschlies et al., 2017). The amplitude of oxygen contribution can be large at tropics because of the oxygen minimum zone with very small pO_2, which amplifies the fractional change. For the models examined in this study, CanESM5 (blue in Figure 4) and GFDL-CM4 (yellow) predict oxygen increase at low latitudes, which is in part compensated by the temperature effect. CNRM-ESM2-1 (red) and IPSL-CM6A-LR (purple) predict oxygen decrease across all latitudes, which reinforces the temperature effect. The ventilation of tropical thermocline is influenced by the complex circulation patterns including zonal jets, wind forcing, mesoscale eddies and

small-scale diapycnal mixing (Brandt et al., 2015; Duteil et al., 2014; Ridder & England, 2014; Gnanadesikan et al., 2007; Thomsen et al., 2016; Lachkar et al., 2018; Shaffer et al., 2000). Climate models cannot fully resolve some of these small scale features and must rely on parameterizations. Furthermore, observations from the tropical Pacific show significant multi-decadal trends that are not well captured by climate models (Stramma et al., 2008; Schmidtko et al., 2017; Ito et al., 2017) which is, at least, partially related to the modes of natural climate varaibility (Duteil et al., 2018; Ito et al., 2019; Deutsch et al., 2011).

Despite the discrepancies in the tropics, the overall scenario dependence is simple and obvious. Comparing the ssp126 to ssp585 scenario, it more than doubles the magnitude of change especially in northern extratropical latitudes (left column in Figure 4) and along the US west coast (Figure 2). While these regions are particularly influenced, moderate decline of metabolic index occurs over much of the Southern Ocean and the subtropical oceans both in the northern and southern hemispheres. For regional application, this calculation can be repeated with different sets of temperature dependence parameters (E) for key species in order to access impacts for a specific ecosystem. Ultimately, the international reduction in the greenhouse gas emissions is fundamental to avoid the continuing, large-scale decline of metabolic constraints in the oceans with biogeochemical, ecological and socio-economic consequences.

Acknowledgments

Datasets for this research are available in the Earth System Grid Federation (ESGF, https://esgf-node.llnl.gov/projects/cmip6/) with these in-text data citation references: CanESM5 (Swart et al., 2019bcdef) licensed under a Creative Commons Attribution ShareAlike 4.0 International License, CNRM-ESM2-1 (Seferian et al., 2019) licensed under a Creative Commons Attribution-NonCommercial-ShareAlike 4.0 International License, GFDL-CM4 (Guo et al., 2018) licensed under a Creative Commons Attribution-ShareAlike 4.0 International License, and IPSL-CM6A-LR (Boucher et al., 2018) licensed under a Creative Commons Attribution-NonCommercial-ShareAlike 4.0 International License. Supplementary Table summerizes the list of ESMs and their reference information. We acknowledge the World Climate Research Programme, which, through its Working Group on Coupled Modelling, coordinated and promoted CMIP6. We thank the climate modeling groups for producing and making available their model output, the ESGF for archiving the data and

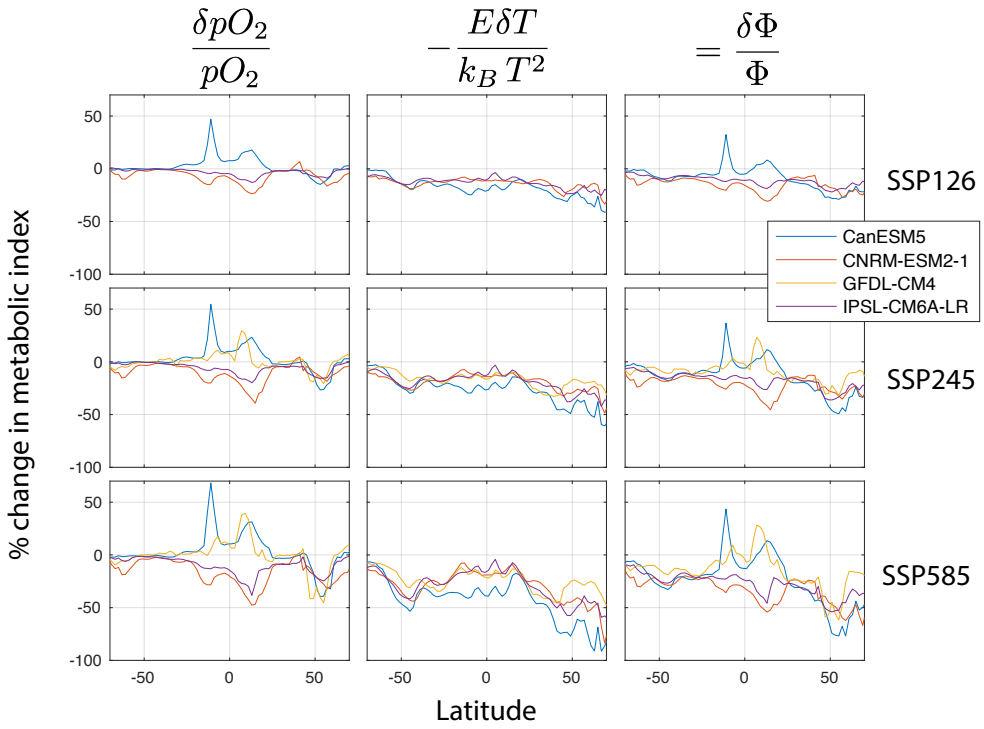

Figure 4. Centennial change of the zonally averaged metabolic index at 200m depth as the difference between the two periods; 1980-2000 and 2080-2100. From left to right, each column shows the contributions from oxygen, temperature, and their combination. From top to bottom, each raw shows the three emission scenarios; ssp126, ssp245 and ssp585. The colors of the line indicate different models; CanESM5 (blue), CNRM-ESM2-1 (red), GFDL-CM4 (yellow), and IPSL-CM6A-LR (purple).

providing access, and the multiple funding agencies who support CMIP6 and ESGF. We are thankful for the funding support from the National Science Foundation, Grant Number OPP-1744755 and OCE-1737188, and acknowledge support from the Cullen-Peck Fellowship at Georgia Institute of Technology.

References

Bopp, L., Resplandy, L., Orr, J. C., Doney, S. C., Dunne, J. P., Gehlen, M., ... Vichi, M. (2013). Multiple stressors of ocean ecosystems in the 21st century: projections with CMIP5 models. *BIOGEOSCIENCES*, *10*(10), 6225-6245. doi: {10.5194/bg-10-6225-2013}

Boucher, O., Denvil, S., Caubel, A., & Foujols, M. A. (2018). *Ipsl ipsl-cm6a-lr model output prepared for cmip6 cmip, downloaded 20190802.* Earth System Grid Federation. Retrieved from `http://cera-www.dkrz.de/WDCC/meta/CMIP6/CMIP6.CMIP.IPSL.IPSL-CM6A-LR` doi: 10.22033/ESGF/CMIP6.1534

Brandt, P., Bange, H. W., Banyte, D., Dengler, M., Didwischus, S. H., Fischer, T., ... Visbeck, M. (2015). On the role of circulation and mixing in the ventilation of oxygen minimum zones with a focus on the eastern tropical North Atlantic. *BIOGEOSCIENCES*, *12*(2), 489-512. doi: {10.5194/bg-12-489-2015}

Cabre, A., Marinov, I., Bernardello, R., & Bianchi, D. (2015). Oxygen minimum zones in the tropical Pacific across CMIP5 models: mean state differences and climate change trends. *BIOGEOSCIENCES*, *12*(18), 5429-5454. doi: {10.5194/bg-12-5429-2015}

Cheng, L., Trenberth, K. E., Fasullo, J., Boyer, T., Abraham, J., & Zhu, J. (2017). Improved estimates of ocean heat content from 1960 to 2015. *Science Advances*, *3*(3). doi: 10.1126/sciadv.1601545

Deutsch, C., Brix, H., Ito, T., Frenzel, H., & Thompson, L. (2011). Climate-Forced Variability of Ocean Hypoxia. *SCIENCE*, *333*(6040), 336-339. doi: {10.1126/science.1202422}

Deutsch, C., Ferrel, A., Seibel, B., Pörtner, H.-O., & Huey, R. B. (2015). Climate change tightens a metabolic constraint on marine habitats. *Science*, *348*(6239), 1132–1135. doi: 10.1126/science.aaa1605

Duteil, O., Boening, C. W., & Oschlies, A. (2014). Variability in subtropical-tropical cells drives oxygen levels in the tropical Pacific Ocean. *GEOPHYSICAL RE-*

SEARCH LETTERS, *41*(24), 8926-8934. doi: {10.1002/2014GL061774}

Duteil, O., Oschlies, A., & Boening, C. W. (2018). Pacific Decadal Oscillation and recent oxygen decline in the eastern tropical Pacific Ocean. *BIOGEOSCIENCES*, *15*(23), 7111-7126. doi: {10.5194/bg-15-7111-2018}

Eddebbar, Y. A., Long, M. C., Resplandy, L., Roedenbeck, C., Rodgers, K. B., Manizza, M., & Keeling, R. F. (2017). Impacts of ENSO on air-sea oxygen exchange: Observations and mechanisms. *GLOBAL BIOGEOCHEMICAL CYCLES*, *31*(5), 901-921. doi: {10.1002/2017GB005630}

Eyring, V., Bony, S., Meehl, G. A., Senior, C. A., Stevens, B., Stouffer, R. J., & Taylor, K. E. (2016). Overview of the coupled model intercomparison project phase 6 (cmip6) experimental design and organization. *Geoscientific Model Development*, *9*(5), 1937–1958. doi: 10.5194/gmd-9-1937-2016

Garcia, H. E., & Gordon, L. I. (1992). Oxygen solubility in seawater: Better fitting equations. *Limnology and Oceanography*, *37*(6), 1307-1312. doi: 10.4319/lo.1992.37.6.1307

Garcia, H. E., Weathers, K., Paver, C. R., Smolyar, I., Boyer, T. P., Locarnini, R. A., ... Reagan, J. R. (2018). World ocean atlas 2018, dissolved oxygen, apparent oxygen utilization, and oxygen saturation. *NOAA Atlas NESDIS*, *3*(83), 38.

Gidden, M. J., Riahi, K., Smith, S. J., Fujimori, S., Luderer, G., Kriegler, E., ... Takahashi, K. (2019). Global emissions pathways under different socioeconomic scenarios for use in cmip6: a dataset of harmonized emissions trajectories through the end of the century. *Geoscientific Model Development*, *12*(4), 1443–1475. doi: 10.5194/gmd-12-1443-2019

Gnanadesikan, A., Russell, J. L., & Zeng, F. (2007). How does ocean ventilation change under global warming? *Ocean Science*, *3*(1), 43–53. doi: 10.5194/os-3-43-2007

Gruber, N. (2011). Warming up, turning sour, losing breath: ocean biogeochemistry under global change. *PHILOSOPHICAL TRANSACTIONS OF THE ROYAL SOCIETY A-MATHEMATICAL PHYSICAL AND ENGINEERING SCIENCES*, *369*(1943), 1980-1996. doi: {10.1098/rsta.2011.0003}

Guo, H., John, J. G., Blanton, C., McHugh, C., Nikonov, S., Radhakrishnan, A., ... Zhao, M. (2018). *Noaa-gfdl gfdl-cm4 model output, downloaded*

20190828. Earth System Grid Federation. Retrieved from `http://cera-www.dkrz.de/WDCC/meta/CMIP6/CMIP6.CMIP.NOAA-GFDL.GFDL-CM4` doi: 10.22033/ESGF/CMIP6.1402

Held, I. M., Guo, H., Adcroft, A., Dunne, J. P., Horowitz, L. W., Krasting, J., ... Zadeh, N. (2019). Structure and performance of GFDL's CM4.0 climate model. *Journal of Advances in Modeling Earth Systems*. doi: 10.1029/2019MS001829

Helm, K. P., Bindoff, N. L., & Church, J. A. (2011). Observed decreases in oxygen content of the global ocean. *GEOPHYSICAL RESEARCH LETTERS*, *38*. doi: {10.1029/2011GL049513}

Ito, T., Long, M. C., Deutsch, C., Minobe, S., & Sun, D. (2019). Mechanisms of Low-Frequency Oxygen Variability in the North Pacific. *GLOBAL BIOGEOCHEMICAL CYCLES*, *33*(2), 110-124. doi: {10.1029/2018GB005987}

Ito, T., Minobe, S., Long, M. C., & Deutsch, C. (2017). Upper ocean O-2 trends: 1958-2015. *GEOPHYSICAL RESEARCH LETTERS*, *44*(9), 4214-4223. doi: {10.1002/2017GL073613}

Keeling, R. F., & Garcia, H. E. (2002). The change in oceanic o2 inventory associated with recent global warming. *PNAS : Proceedings of the National Academy of Sciences of the United States of America.*, *99*(12), 7848–7853.

Keeling, R. F., Krtzinger, A., & Gruber, N. (2010). Ocean deoxygenation in a warming world. *Annual Review of Marine Science*, *2*(1), 199-229. (PMID: 21141663) doi: 10.1146/annurev.marine.010908.163855

Lachkar, Z., Levy, M., & Smith, S. (2018). Intensification and deepening of the Arabian Sea oxygen minimum zone in response to increase in Indian monsoon wind intensity. *BIOGEOSCIENCES*, *15*(1), 159-186. doi: {10.5194/bg-15-159-2018}

Matear, R. J., Hirst, A. C., & McNeil, B. I. (2000). Changes in dissolved oxygen in the southern ocean with climate change. *Geochemistry, geophysics, geosystems*, *1*(11).

Oschlies, A., Brandt, P., Stramma, L., & Schmidtko, S. (2018). Drivers and mechanisms of ocean deoxygenation. *Nature Geoscience*, *11*(7), 467–473. doi: 10.1038/s41561-018-0152-2

Oschlies, A., Duteil, O., Getzlaff, J., Koeve, W., Landolfi, A., & Schmidtko, S.

(2017). Patterns of deoxygenation: sensitivity to natural and anthropogenic drivers. *PHILOSOPHICAL TRANSACTIONS OF THE ROYAL SOCIETY A-MATHEMATICAL PHYSICAL AND ENGINEERING SCIENCES*, *375*(2102). doi: {10.1098/rsta.2016.0325}

Ridder, N. N., & England, M. H. (2014). Sensitivity of ocean oxygenation to variations in tropical zonal wind stress magnitude. *GLOBAL BIOGEOCHEMICAL CYCLES*, *28*(9), 909-926. doi: {10.1002/2013GB004708}

Schmidtko, S., Stramma, L., & Visbeck, M. (2017). Decline in global oceanic oxygen content during the past five decades. *NATURE*, *542*(7641), 335+. doi: {10.1038/nature21399}

Seferian, R. (2018). *Cnrm-cerfacs cnrm-esm2-1 model output prepared for cmip6 cmip, downloaded 20191006.* Earth System Grid Federation. Retrieved from `https://doi.org/10.22033/ESGF/CMIP6.1391` doi: 10.22033/ESGF/CMIP6.1391

Shaffer, G., Leth, O., Ulloa, O., Bendtsen, J., Daneri, G., Dellarossa, V., ... Sehlstedt, P. (2000). Warming and circulation change in the eastern South Pacific Ocean. *GEOPHYSICAL RESEARCH LETTERS*, *27*(9), 1247-1250.

Stramma, L., Johnson, G. C., Sprintall, J., & Mohrholz, V. (2008). Expanding oxygen-minimum zones in the tropical oceans. *SCIENCE*, *320*(5876), 655-658. doi: {10.1126/science.1153847}

Stramma, L., Oschlies, A., & Schmidtko, S. (2012). Mismatch between observed and modeled trends in dissolved upper-ocean oxygen over the last 50 yr. *BIOGEOSCIENCES*, *9*(10), 4045-4057. doi: {10.5194/bg-9-4045-2012}

Swart, N. C., Cole, J. N., Kharin, V. V., Lazare, M., Scinocca, J. F., Gillett, N. P., ... Sigmond, M. (2019b). *Cccma canesm5 model output prepared for cmip6 cmip historical, version 20190306.* Earth System Grid Federation. Retrieved from `http://cera-www.dkrz.de/WDCC/meta/CMIP6/CMIP6.CMIP.CCCma.CanESM5.historical` doi: 10.22033/ESGF/CMIP6.3610

Swart, N. C., Cole, J. N., Kharin, V. V., Lazare, M., Scinocca, J. F., Gillett, N. P., ... Sigmond, M. (2019c). *Cccma canesm5 model output prepared for cmip6 cmip picontrol, version 20190429.* Earth System Grid Federation. Retrieved from `http://cera-www.dkrz.de/WDCC/meta/CMIP6/CMIP6.CMIP.CCCma.CanESM5.piControl` doi: 10.22033/ESGF/CMIP6.3673

Swart, N. C., Cole, J. N., Kharin, V. V., Lazare, M., Scinocca, J. F., Gillett, N. P., ... Sigmond, M. (2019d). *Cccma canesm5 model output prepared for cmip6 scenariomip ssp126, version 20190429.* Earth System Grid Federation. Retrieved from `http://cera-www.dkrz.de/WDCC/meta/CMIP6/CMIP6.ScenarioMIP.CCCma.CanESM5.ssp126` doi: 10.22033/ESGF/CMIP6.3683

Swart, N. C., Cole, J. N., Kharin, V. V., Lazare, M., Scinocca, J. F., Gillett, N. P., ... Sigmond, M. (2019e). *Cccma canesm5 model output prepared for cmip6 scenariomip ssp245, version 20190429.* Earth System Grid Federation. Retrieved from `http://cera-www.dkrz.de/WDCC/meta/CMIP6/CMIP6.ScenarioMIP.CCCma.CanESM5.ssp245` doi: 10.22033/ESGF/CMIP6.3685

Swart, N. C., Cole, J. N., Kharin, V. V., Lazare, M., Scinocca, J. F., Gillett, N. P., ... Sigmond, M. (2019f). *Cccma canesm5 model output prepared for cmip6 scenariomip ssp585, version 20190429.* Earth System Grid Federation. Retrieved from `http://cera-www.dkrz.de/WDCC/meta/CMIP6/CMIP6.ScenarioMIP.CCCma.CanESM5.ssp585` doi: 10.22033/ESGF/CMIP6.3696

Swart, N. C., Cole, J. N. S., Kharin, V. V., Lazare, M., Scinocca, J. F., Gillett, N. P., ... Winter, B. (2019a). The canadian earth system model version 5 (CanESM5.0.3). *Geoscientific Model Development*, *12*(11), 4823–4873. doi: 10.5194/gmd-12-4823-2019

Sfrian, R., Nabat, P., Michou, M., Saint-Martin, D., Voldoire, A., Colin, J., ... Madec, G. (2019). Evaluation of cnrm earth system model, CNRM-ESM2-1: Role of earth system processes in present-day and future climate. *Journal of Advances in Modeling Earth Systems*. doi: 10.1029/2019MS001791

Tagklis, F., Bracco, A., & Ito, T. (2017). Physically driven patchy o2 changes in the north atlantic ocean simulated by the cmip5 earth system models. *Global Biogeochemical Cycles*, *31*(8), 1218-1235. doi: 10.1002/2016GB005617

Takano, Y., Ito, T., & Deutsch, C. (2018). Projected Centennial Oxygen Trends and Their Attribution to Distinct Ocean Climate Forcings. *GLOBAL BIOGEOCHEMICAL CYCLES*, *32*(9), 1329-1349. doi: {10.1029/2018GB005939}

Thomsen, S., Kanzow, T., Colas, F., Echevin, V., Krahmann, G., & Engel, A. (2016). Do submesoscale frontal processes ventilate the oxygen minimum zone off Peru? *GEOPHYSICAL RESEARCH LETTERS*, *43*(15), 8133-8142. doi: {10.1002/2016GL070548}

Zanna, L., Khatiwala, S., Gregory, J. M., Ison, J., & Heimbach, P. (2019). Global reconstruction of historical ocean heat storage and transport. *Proceedings of the National Academy of Sciences*, *116*(4), 1126–1131. doi: 10.1073/pnas.1808838115